RSC Advances

PAPER

View Article Online
View Journal | View Issue

Cite this: *RSC Adv.*, 2014, **4**, 36923

Effects of a disulfide bridge prior to amyloid formation of the ABRI peptide†

Jorge A. Ceballos,[b] Marco A. Giraldo[b] and Pilar Cossio*[a]

Received 11th February 2014
Accepted 31st July 2014

DOI: 10.1039/c4ra06034b

www.rsc.org/advances

The ABRI peptide is involved in the neurodegenerative disease Familial British Dementia, which has its origin in the misfolding of the peptide. Characterizing the most probable conformations of the monomer in solution can provide insights into how misfolding could occur in the steps prior to aggregation. Specifically, we analyzed the structural effects caused by the formation of a single disulfide bond, which has been reported to be important in amyloid assembly. We used all-atom molecular dynamics simulations with an enhanced sampling technique to obtain the lowest free energy conformations for two cases: the peptide with and without the disulfide bond between residues 5Cys and 22Cys. Bulk measurements on the conformations agree with experiments by elucidating ABRI as a disordered peptide. We find remarkable differences at the microscopic level between the most probable structures; with the disulfide bond the peptide is compact and α-helical, without the bond it is partially extended with slight β-bridges.

1 Introduction

Familial British Dementia (FBD) is a neurodegenerative disease which causes dementia and is similar to Alzheimer's and Parkinson's disease, among others.[1] These diseases are caused by the misfolding of a protein into a pathological state, where it does not perform its biological function and forms insoluble fibrillar amyloids, mostly in brain tissue.[2] The cause of misfolding is still an open problem and these diseases have no definite cure. Nevertheless, experimental and therapeutic methods may be employed to further our understanding of amyloid formation. Currently, antibodies and inhibitors are successfully being used as preventative/therapeutic medicines.[1,3–5] Theory and computer simulations also provide detailed information concerning initial states, nucleation steps to aggregation,[6–11] and the effects of disulfide bonds on oligomers.[12,13]

The core peptide involved in FBD, denominated ABRI, is quite small, containing only 34 amino acids, and has its origin in a single nucleotide mutation of the stop-codon in the BRI gene. This mutation generates a longer reading frame and adds 11 extra amino acids to BRI2,[14] a type II transmembrane protein. BRI2 is cleaved by the prohormone convertase furin[15] and, in wild-type conditions, a soluble peptide containing 23 amino acids is released. The mutated form of the ABRI peptide is deposited in the extracellular membrane generating amyloid fibrils, which cause neuronal dysfunction and dementia.[14]

Previous experimental studies have established the importance of the disulfide bond (SS-bond) formed between the peptide's residues, 5Cys and 22Cys.[16–20] This bond can be either intra- or inter-molecular depending on the environmental conditions. Due to the peptide's location in the extracellular tissue, a possibility is that the disulfide bond is intra-molecular. However, in the absence of reducing agents, the bond might be inter-molecular and may form disulfide-bonded multimer amyloids. The aggregation effects of oxidized and reduced ABRI (with and without the SS-bond, respectively) have been studied, over long incubation times, for different pH and molecular concentrations. These studies suggest that ABRI aggregation and protofibril formation are very pH-dependent, and at slightly basic pH (8–10) the 5Cys–22Cys disulfide bond is scrambled, leading to the formation of covalently linked inter-molecular aggregates.[21] Circular dichroism (CD) measurements show that, after prolongated incubation times (∼weeks), both forms of reduced and oxidized ABRI have a tendency to adopt β-structure aggregates at neutral pH.[17,22] However, when identical studies were conducted with reducing agents (such as 1 mM cysteine) the CD signal showed no peptide precipitation, indicating the importance of disulfide bond formation for aggregation.[23] For short incubation times (∼minutes), CD experiments showed that the conformational weighted average of oxidized ABRI is predominantly disordered at neutral pH.[21] However, robust structural characterization of the ABRI monomer is still lacking. Ideally, one would like to obtain X-ray or NMR structures to characterize the structural ensemble prior to aggregation,

[a]*Department of Theoretical Biophysics, Max Planck Institute of Biophysics, 60438 Frankfurt am Main, Germany. E-mail: pilar.cossio@biophys.mpg.de; Fax: +49 (0)69 6303-4502; Tel: +49 (0)69 6303-0*

[b]*Institute of Physics, University of Antioquia, Calle 70 No. 52-21. A.A.1226, Medellín, Colombia*

† Electronic supplementary information (ESI) available. See DOI: 10.1039/c4ra06034b

unfortunately, this is quite difficult mainly due to the peptide's flexibility. Several homology models of ABRI suggest a predominant β-sheet structure,[17,23] but they do not propose a proper conformational ensemble or take into account the formation (or absence) of the disulfide bond.

In contrast to homology-based studies, we use molecular dynamics (MD) simulations as a "microscope" into the atomic world. Together with an enhanced sample method, we obtain converged probability distributions of the configurations of oxidized and reduced monomeric ABRI. We find substantial differences between the most populated structures. Our results indicate that the peptide without the disulfide bond, which is mostly non-compact and flexible, is prone to initial β-content formation and could possibly be easier to initiate aggregation.

2 Methods

The initial conformation of the ABRI peptide, with the primary sequence EASNCFAIRHFENKFAVETLICSRTVKKNIIEEN, was built in a completely unfolded state using the xLeap tool of the AMBER package.[24] The peptide was introduced in a cubic-box of 321.42 nm^3 (68.5 Å per edge) with 10 242 water molecules. A large box permits the enhanced sampling method to fully explore the conformational space, limited by the protein adopting unfolded states. No extra ions were needed to achieve electroneutrality. Periodic boundary conditions were applied. The AMBER99SB-ILDN[25] and TIP3P[26] force fields were used for the protein and water molecules, respectively. The particle-mesh Ewald method[27] was used for the long-range electrostatics with a cut-off of 0.9 nm, as well as for the short-range neighbor list. The radius cut-off for the Lennard-Jones potential was 1 nm. Temperature coupling was done through the Nosé–Hoover thermostat,[28,29] and the Andersen–Parrinello–Rahman scheme[30] was used for isotropic pressure coupling to 1 bar. MD simulations ran with the Gromacs software,[31] and the final time step was 2 fs. Energy minimization ran for 100 000 steps at 0 K, then the system was heated to its final temperature, 300 K, by increasing intervals of 50 K for 50 ps each. MD equilibration was done for 10 ns at 300 K.

To avoid getting trapped in local energy minima, we used an enhanced sampling method, bias exchange metadynamics (BEM),[32] to extensively explore the conformational space and obtain the free energy population of the system. Since the initial configuration of the peptide was completely unfolded, and our interest is to characterize it with and without the disulfide bridge, we first performed a broad BEM simulation to obtain conformations where the Cys residues were in contact (details are provided in the ESI†). A conformation with contacting 5Cys–22Cys was selected randomly from a wide sample, and was the starting configuration of our two main BEM studies, which differed only in the presence (or absence) of the disulfide bond. The SS-bond was represented as an additional harmonic-bond restraint over the two sulfur atoms of the Cys residues, with a binding constant of 10 000 kJ and an equilibrium position at 2.5 Å. The simulation without the SS-bond had no restraint over these atoms. All other parameters and initial conditions were identical for both simulations. The PLUMED package[33] was used to run the BEM methodology. Both simulations were used to run BEM over 12 replicas of the system, 11 of which biased a different Ψ dihedral angle of the peptide, corresponding to 6F, 8I, 10H, 12E, 14K, 16A, 18E, 20L, 23S, 25T, and 27K, with periodicity in $[-\pi,\pi]$. This collective variable (CV) setup was chosen in a similar way to previous studies.[34] The biasing Gaussians were deposited every steps of 10 ps, with a height of 1.5 kJ and width equal to the standard deviation of the CV's value in an unbiased MD run. Biasing potentials were exchanged every 40 ps following the BEM protocol.[32,35] Each replica ran for 88 ns, giving a total simulation time of ~1 μs for each of the BEM studies (with and without the SS-bond).

The METAGUI tool[36] was used to analyze the convergence and obtain the lowest free energy conformations of the system. Convergence was found after 35 ns by analyzing the evolution of the free energy profiles. As an example of convergence, in Fig. 1 we present the free energy profiles of several dihedral angles calculated for the first half (black line) and second half (red line) of the trajectories after a filling time of 35 ns, for the setup without the SS-bond. The calculated profiles are very alike within ~1 kcal mol^{-1} of error (blue line Fig. 1), and similar results were found for the other CVs and BEM simulations. To obtain the lowest free energy structures, the BEM trajectory frames were grouped into clusters in a collective variable space.[37] 9 CVs corresponding to the dihedral angles Ψ of residues 6F, 8I, 10H, 12E, 14K, 16A, 18E, 20L, and 23S were used for clustering with a grid spacing of 1.04 rad and periodicity in $[-\pi,\pi]$. Frames belonging to each cluster are structurally similar within 3 Å of RMSD of the C_α atoms. The free energy of each cluster was estimated by a weighted-histogram approach.[37,38] The analysis was done for two different filling times and the correlated free energies confirm the convergence of the results (ESI Fig. 1†). The clustering and free energy analysis were identical for both disulfide bond studies.

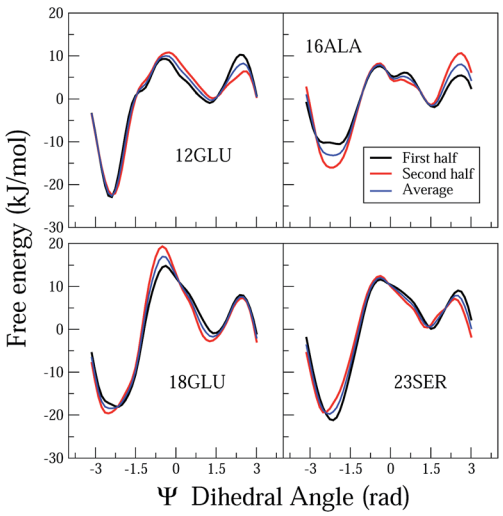

Fig. 1 Calculated free energy profiles of Ψ dihedral angles for the first half (black line) and second half (red line) of the trajectories after a filling time of 35 ns. The profiles shown are for residues 12GLU, 16ALA, 18GLU and 23SER, for the setup without the disulfide bond. The average profile within ~1 kcal mol^{-1} of error is shown in blue.

3 Results

Fig. 2 shows representative structures belonging to the most populated cluster of the ABRI peptide in solution, for two different cases: BEM simulations with and without a disulfide bond between residues 5Cys and 22Cys. We find that the most probable structures for oxidized ABRI are compact with an α-helix between residues 18 to 26, and hydrophobic residues are mostly buried in the core of the peptide (left column Fig. 2). Two salt bridges are found between residues 14K-18E, and 2E-28K. In contrast, reduced ABRI structures are less compact with a β-bridge component, and the hydrophobic residues are slightly more exposed to the solvent (right column Fig. 2). Sulfur atoms are at an average distance of 7.8 Å, and a salt-bridge is found between residues 9R and 32E. Both peptide forms present a flexible region in their last 11 residues (C-terminus), corresponding to the amino acids that are added in the mutated protein form of patients with FBD disease. This flexibility might be due to the large number of charged residues in the tail (5 out of 11).

To gain insight into the differences between the two most probable states, in Fig. 3 we plot the two-dimensional ϕ,Ψ dihedral angle probability distribution (Ramachandran plot) for oxidized and reduced ABRI. We find that the oxidized form has its global maximum around $\phi \approx -65°$, $\Psi \approx -45°$ which corresponds to the α-helical region, whereas reduced ABRI has its maximum near $\phi \approx -70°$, $\Psi \approx 130°$ located within the β-structure region of the Ramachandran plot (red arrows in Fig. 3). In the ESI Fig. 2† (top), for each dihedral angle pair, we compare the values of these two distributions by calculating the *Z*-score of their difference with respect to the mean difference over the full set. *P*-values of the areas of the Ramachandran plot at a threshold of 5% (two-tail) significance are shown in ESI Fig. 2† (bottom). Distinct features are found between the α-helical preference with the SS-bond in comparison to the β-like character when it is broken. Even though the two distributions substantially differ, we note that most of the residues do not form a secondary structure and have no overall effect.

To further characterize the structural properties caused by the effect of the disulfide bond on the most relevant states, we calculated several observables, such as the radius of gyration, exposed hydrophobic surface area, and secondary structure content. We completed this analysis for structures belonging to the 20 lowest free energy clusters of each BEM simulation. The average value of the observable $\mathcal{O}$ is calculated as $\langle \mathcal{O} \rangle = \sum_i \mathcal{O}_i e^{-F_i/k_B T}$, where i is the cluster index and F_i is the free energy of cluster i calculated with a WHAM approach (see Methods). We find notable differences between the structural observables for the two simulations. Fig. 4A shows the distribution of the solvent accessible surface area (SASA) of the hydrophobic residues of ABRI with and without the SS-bond (black and blue distributions, respectively). Hydrophobic residues of oxidized ABRI are less exposed to the solvent than those

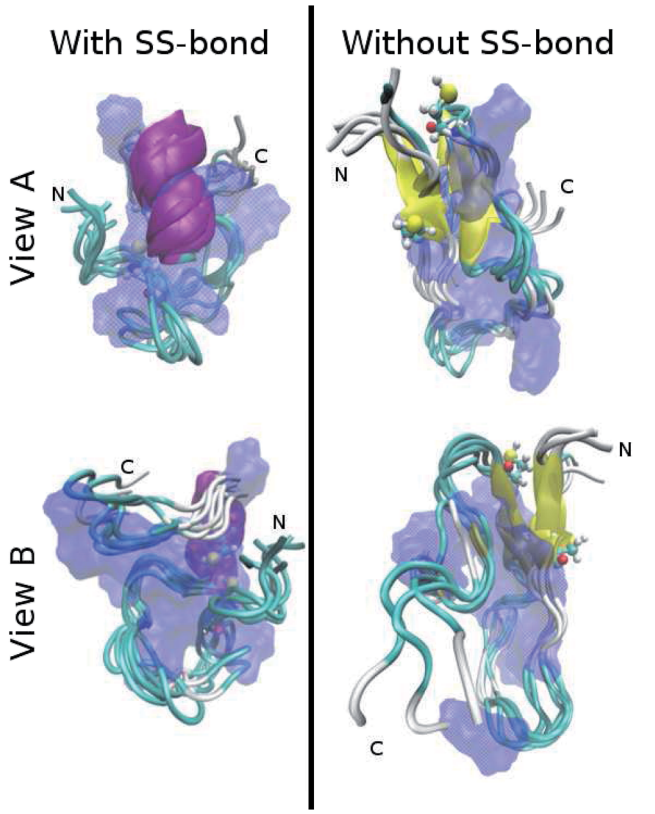

Fig. 2 Lowest free energy cluster of the ABRI peptide with (left) and without (right) the disulfide bond between residues 5Cys and 22Cys. Secondary structure content is shown as *new-cartoon* representation, α-helices are shown in violet and β-sheets in yellow. Hydrophobic residues are in transparent blue, and atoms of Cys residues are shown as spheres. Two different views (A and B) are shown for each. N and C indicate the peptide's termini.

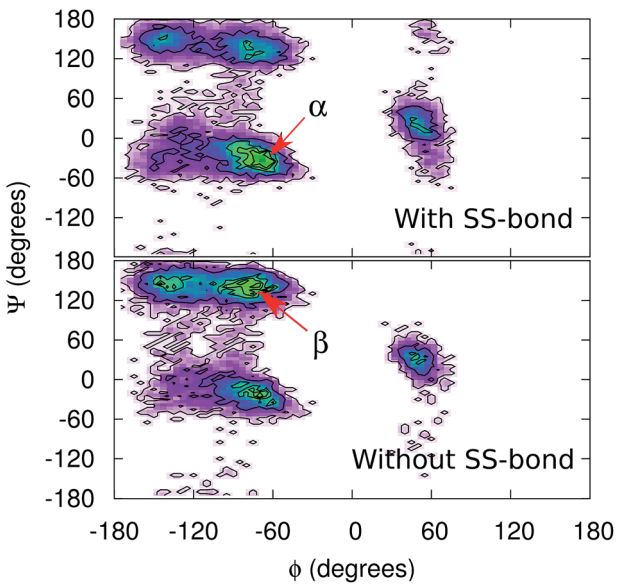

Fig. 3 Normalized probability distribution of the ϕ, Ψ dihedral angle (Ramachandran plot) for oxidized (top) and reduced (bottom) ABRI. Arrows indicate the global maximum for each distribution, and the corresponding secondary structure element.

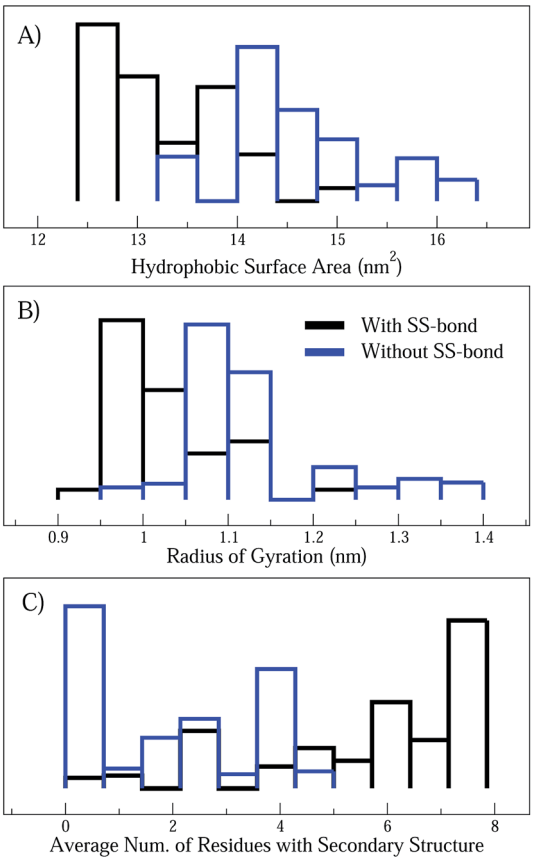

Fig. 4 Probability distributions of the (A) hydrophobic surface area (nm^2), (B) radius of gyration (nm), and (C) number of residues in the secondary structure. Results for the simulations of oxidized and reduced ABRI are shown in black and blue colors, respectively. Distributions are calculated over the 20 most probable clusters of each simulation.

in the reduced form, with an average hydrophobic SASA of 13.21 and 14.45 nm^2, respectively. This is consistent with the fact that structures with the SS-bond are more compact. Probability distributions of the radius of gyration are shown in Fig. 4B, average values are 1.01 and 1.13 nm, respectively for oxidized and reduced ABRI. In Fig. 4C, we present the distribution of the average number of residues in the secondary structure, calculated using the DSSP tool.[39] Oxidized ABRI has more residues in the secondary structure elements than in the reduced form, with average values of ~6 and ~2 residues, respectively. This result also indicates that, for both disulfide bond conformations, the secondary content is low with most residues being unstructured. Interestingly, residues in the secondary elements are α-helical when the SS-bond is formed whereas residues are predominantly found in β-bridges in the absence of the SS-bond (as shown in Fig. 2 and 3 for the most populated cluster). The breakage of the disulfide bond could induce an α to β transition in the initial steps of aggregation, as reported for other amyloidogenic peptides.[40] This hypothesis should be confirmed with accurate and convergent free energy calculations from the oxidized to the reduced folded state. However, to obtain preliminary insights into the stability of the α-helical state in the local thermodynamic basin, we performed several unbiased MD simulations starting from the most probable conformation of oxidized ABRI (left column Fig. 2) with and without the SS-bond. In the ESI, Fig. 3A,† we present the root-mean-square-deviation (RMSD) from the initial configuration as a function of time for three simulations each with or without the disulfide bond. We find that if the disulfide bond is broken, after ~8 ns the configurations have a larger RMSD to the initial structure than in the oxidized form, indicating that there is a less stable thermodynamic basin if no SS-bond is present. This is also confirmed in the ESI, Fig. 3B,† by comparing the probability distributions of the RMSD after 20 ns of simulation time in both ABRI forms.

So far we have described the microscopic picture of ABRI's conformational states, with small but notable differences between its most probable structures in the oxidized or reduced form. Ideally, one would like to compare these computational results with a variety of experiments such as NMR and CD spectroscopy of the peptide under the conditions simulated. However, few experimental studies are available in these conditions, mainly, because the purified ABRI peptide has limited solubility in aqueous solution at neutral pH. This insolubility is mostly attributed to the high aggregation state of the dry ABRI peptide (pre-existing "seed") before dissolution. Nevertheless, in ref. 21 CD spectra of oxidized ABRI at 5 μM concentration, pH 6.9 and 7.8, after 5 min of incubation time are presented. Both experimental spectra show a sharp minimum around 198 nm indicating a disordered-like conformation. We used the DichroCalc[41] program for calculating the theoretical CD spectra from the most probable ABRI configurations, and also from several structural classes of α, β and random-coil PDB structures. The results are shown in the ESI, Fig. 4.† We find that both ABRI forms present similar theoretical CD spectra as those of random-coil/disordered proteins, and differ significantly from those of α-helical or β proteins. However, as mentioned in ref. 42 and 43 the parameters for calculating the CD spectra of random-coil proteins are not yet completely optimized and the sign of the peak is wrong (ESI Fig. 4†). Thus, we are limited to only a qualitative comparison with both the theory and experiments consistently suggesting a predominantly disordered structure to the ABRI peptide under the conditions simulated. These results are in agreement with the low number of residues found in the secondary structure elements (Fig. 4C).

Whereas a single bulk measurement presents a hazy picture of ABRI as a random-coil, with our computational study we demonstrated the importance of having a detailed microscopic description to elucidate the differences between oxidized and reduced ABRI. The atomic picture suggests a possible initial mechanism towards aggregation from an α-helical state into a β-forming structure when the disulfide bond is broken.

4 Conclusions

The intrinsic flexibility of the peptides involved in neurodegenerative diseases render their experimental characterization quite difficult. Here, we used sophisticated computational tools

to obtain the conformational ensemble of the ABRI peptide involved in Familial British Dementia. Specifically, we studied the effects of the formation, and absence, of a disulfide bond between residues 5Cys and 22Cys. We find significant differences between the most populated states of the oxidized and reduced ABRI. If a disulfide bond is formed, conformations are compact, with an α-helical component and a hydrophobic core. On the other hand, if the disulfide bond is broken, the main configurations are expanded, have more solvent exposed hydrophobic residues, and have slight β secondary structure components. For both cases, with and without the SS-bond, the residues are mostly unstructured, and the last 11 amino acids (those added in the mutated form) are very flexible. These results are consistent with the available experimental CD spectra at similar conditions,[21] which suggest that the early stages of monomeric ABRI may be best characterized as a disordered peptide. However, the detailed atomic description of the structural ensembles confirm the relevance of disulfide bonds in amyloidogenic peptides.[18] Our analysis suggests that reduced ABRI has a set of characteristics, such as exposed hydrophobic residues and β-secondary structure, that have been suggested to facilitate polymeric assembly and agglomeration.[1,44] However, we have only structurally characterized monomeric ABRI in solution, and further simulations of dimers, trimers and multimers,[6] including all possible permutations of the disulfide bonds (such as in ref. 12 and 13) are still needed to obtain a clear idea of the general mechanism of amyloidogenesis. Moreover, monitoring the effects of pyroglutamate residues[20] might also be of fundamental relevance.

Acknowledgements

The authors acknowledge Dr. Gareth Bland for useful help with the statistics and revising of the manuscript. PC was supported by the Max Planck society, and simulations were performed in the Centro Regional de Simulación y cálculo Avanzado (CRESCA) of the University of Antioquia.

References

1 F. Chiti and C. M. Dobson, *Annu. Rev. Biochem.*, 2006, **75**, 333–366.
2 T. Revesz, J. Ghiso, T. Lashley, G. Plant, A. Rostagno, B. Frangione and J. Holton, *J. Neuropathol. Exp. Neurol.*, 2003, **62**, 885–898.
3 D. C. Rubinsztein, *Nature*, 2006, **443**, 780–786.
4 M. Frugier, T. Bour, M. Ayach, M. A. Santos, J. Rudinger-Thirion, A. Théobald-Dietrich and E. Pizzi, *FEBS Lett.*, 2010, **584**, 448–454.
5 A. Chilumuri, M. Odell and N. G. N. Milton, *ACS Chem. Neurosci.*, 2013, **4**, 1501–1512.
6 F. Baftizadeh, F. Pietrucci, X. Biarnes and A. Laio, *Phys. Rev. Lett.*, 2013, **110**, 168103.
7 B. Ma and R. Nussinov, *Proc. Natl. Acad. Sci. U. S. A.*, 2002, **99**, 14126–14131.
8 S. Auer, C. M. Dobson, M. Vendruscolo and A. Maritan, *Phys. Rev. Lett.*, 2008, **101**, 258101.
9 L. Larini and J.-E. Shea, *Biophys. J.*, 2012, **103**, 576–586.
10 G. Rossetti, P. Cossio, A. Laio and P. Carloni, *FEBS Lett.*, 2011, **585**, 3086–3089.
11 D. Thirumalai, D. Klimov and R. Dima, *Curr. Opin. Struct. Biol.*, 2003, **13**, 146–159.
12 Y. Chen and N. Dokholyan, *J. Mol. Biol.*, 2005, **354**, 473–482.
13 S. Cho, Y. Levy, J. Onuchic and P. Wolynes, *Phys. Biol.*, 2005, **2**, S44–S55.
14 R. Vidal, B. Frangione, A. Rostagno, S. Mead, T. Revesz, G. Plant and J. Ghiso, *Nature*, 1999, **399**, 776–781.
15 T. Lashley, T. Revesz, G. Plant, R. Bandopadhyay, A. J. Lees, B. Frangione, N. W. Wood, R. de Silva, J. Ghiso, A. Rostagno and J. L. Holton, *Neuropathol. Appl. Neurobiol.*, 2008, **34**, 492–505.
16 O. El-Agnaf, S. Nagala, B. Patel and B. Austen, *J. Mol. Biol.*, 2001, **310**, 157–168.
17 O. El-Agnaf, J. M. Sheridan, C. Sidera, G. Siligardi, R. Hussain, P. I. Haris and B. M. Austen, *Biochemistry*, 2001, **40**, 3449–3457.
18 Y. Li, J. Yan, X. Zhang and K. Huang, *Proteins: Struct., Funct., Bioinf.*, 2013, **81**, 1862–1873.
19 R. Srinivasan, R. Marchant and M. Zagorski, *Amyloid*, 2004, **11**, 10–13.
20 A. Saul, T. Lashley, T. Revesz, J. Holton, J. A. Ghiso, J. Coomaraswamy and O. Wirths, *Neurobiol. Aging*, 2013, **34**, 1416–1425.
21 R. Srinivasan, E. M. Jones, K. Liu, J. Ghiso, R. E. Marchant and M. G. Zagorski, *J. Mol. Biol.*, 2003, **333**, 1003–1023.
22 V. Lelyveld, O. El-Agnaf, G. Siligardi, R. Hussain, P. I. Haris, M. Lee and B. Austen, *J. Spectrosc.*, 2001, **15**, 129–139.
23 D. Mahadevan, T. Chattopadhyay, R. A. P. R. O. Brien and J. W. Saldanha, *Protein Pept. Lett.*, 2001, **8**, 139–146.
24 D. A. Case, T. E. Cheatham, T. Darden, H. Gohlke, R. Luo, K. M. Merz, A. Onufriev, C. Simmerling, B. Wang and R. J. Woods, *J. Comput. Chem.*, 2005, **26**, 1668–1688.
25 K. Lindorff-Larsen, S. Piana, K. Palmo, P. Maragakis, J. L. Klepeis, R. O. Dror and D. E. Shaw, *Proteins: Struct., Funct., Bioinf.*, 2010, **78**, 1950–1958.
26 W. L. Jorgensen, J. Chandrasekhar, J. D. Madura, R. W. Impey and M. L. Klein, *J. Chem. Phys.*, 1983, **79**, 926–935.
27 T. A. Darden and D. York, *J. Chem. Phys.*, 1993, **98**, 10089.
28 S. Nose, *Mol. Phys.*, 1984, **52**, 255–268.
29 W. G. Hoover, *Phys. Rev. A: At., Mol., Opt. Phys.*, 1985, **31**, 1695.
30 M. Parrinello and A. Rahman, *Phys. Rev. Lett.*, 1980, **45**, 1196.
31 B. Hess, C. Kutzner, D. van der Spoel and E. Lindahl, *J. Chem. Theory Comput.*, 2008, **4**, 435–447.
32 S. Piana and A. Laio, *J. Phys. Chem. B*, 2007, **111**, 4553–4559.
33 M. Bonomi, D. Branduardi, G. Bussi, C. Camilloni, D. Provasi, P. Raiteri, D. Donadio, F. Marinelli, F. Pietrucci, R. A. Broglia and M. Parrinello, *Comput. Phys. Commun.*, 2009, **180**, 1961–1972.
34 S. Grigoriu, R. Bond, P. Cossio, J. A. Chen, N. Ly, G. Hummer, R. Page, M. S. Cyert and W. Peti, *PLoS Biol.*, 2013, **11**, 1001492.
35 P. Cossio, F. Marinelli, A. Laio and F. Pietrucci, *J. Phys. Chem. B*, 2010, **114**, 3259–3265.

36 F. M. Xevi Biarnés, F. Pietrucci and A. Laio, *Comput. Phys. Commun.*, 2012, **183**, 203–211.
37 F. Marinelli, F. Pietrucci, A. Laio and S. Piana, *PLoS Comput. Biol.*, 2009, **5**, e100045.
38 S. Kumar, J. M. Rosenberg, D. Bouzida, R. H. Swendsen and P. A. Kollman, *J. Comput. Chem.*, 1995, **16**, 1339–1350.
39 W. Kabsch and C. Sander, *Biopolymers*, 1983, **22**, 2577–2637.
40 K. M. Pam, M. Baldwin, J. Nguyen, M. Gasset, A. Serban, D. Groth, I. Mehlhorn, Z. Huang, R. Fletterick, F. Cohen and S. Prusiner, *Proc. Natl. Acad. Sci. U. S. A.*, 1993, **90**, 10962–10966.
41 B. M. Bulheller and J. D. Hirst, *Bioinformatics*, 2009, **25**, 539–540.
42 J. Hirst, S. Bhattacharjee and A. Onufriev, *Faraday Discuss.*, 2003, **122**, 253–267.
43 B. M. Bulheller, A. Rodger and J. D. Hirst, *Phys. Chem. Chem. Phys.*, 2007, **9**, 2020–2035.
44 V. N. Uversky, *Curr. Alzheimer Res.*, 2008, **5**, 260–287.